

El Niño and the Southern Oscillation (ENSO)

The previous chapter stressed the importance of the tropics for the coupling between ocean and atmosphere and showed how positive feedback between the sea surface temperature (SST) and the atmospheric convection zones can result in rapid magnifications of initially small disturbances. We now continue this theme and examine in detail the situation in the tropical Pacific Ocean. This region is characterized by very high sea surface temperatures and extremely low zonal temperature gradients in the west (the so-called "warm pool"; see Figure 2.5a); small SST variations in this region can grow into interannual climate variations of global proportions.

We start by looking at some observations. It is well known that climate conditions in the Australian continent vary between the extremes of devastating droughts and equally devastating floods. In eastern Australia, years of severe drought have been documented for nearly two centuries, and it has been noticed that they come at irregular intervals of a few years. We know now that they are part of a global phenomenon known as the El Niño - Southern Oscillation, or ENSO, phenomenon, which manifests itself in fluctuations of rainfall, winds, ocean currents, and sea surface temperature of the tropical oceans, and of the Pacific Ocean in particular. If these fluctuations were strictly periodic people would probably have learnt to plan for their occurrence. What makes them so difficult to cope with is their irregularity. As it is, the ENSO affects national economies often in an unpredictable manner, causing great hardship and social upheaval and at least on one occasion the downfall of a government (Tomczak, 1981a). The data shown in Figure 19.1

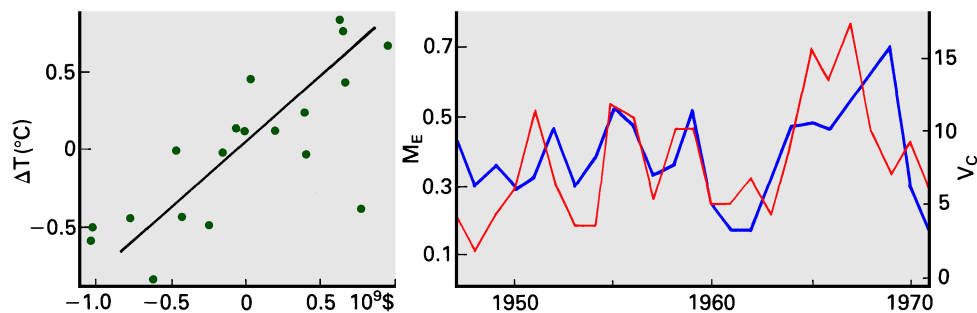


Fig. 19.1. Examples of the impact of climate variability on economic activity. (a) Anomalies of sea surface temperature (SST) in northern Australian winter (June-August, 5° - 15°S , 120° - 160°E) against variations in aggregate value of five Australian crops (wheat, barley, oats, sugar cane, and potatoes) in the subsequent summer, after removal of long-term trends due to productivity. Low SST is associated with drought; the regression line indicates a decrease of 1 billion \$ for a 1°C decrease in SST. (b) Variations in wind intensity along the coast of Oregon, as measured by the mean offshore Ekman transport M_E during April to September ($\text{m}^2 \text{s}^{-1}$ per m of coastline, left scale and thin line), and variations in the catch of Dungeness crab (V_C , in million pounds, right scale and thick line) eighteen months later. The total catch reflects upwelling conditions remarkably well. (The time scale is correct for M_E but shifted by 18 months for V_C .)

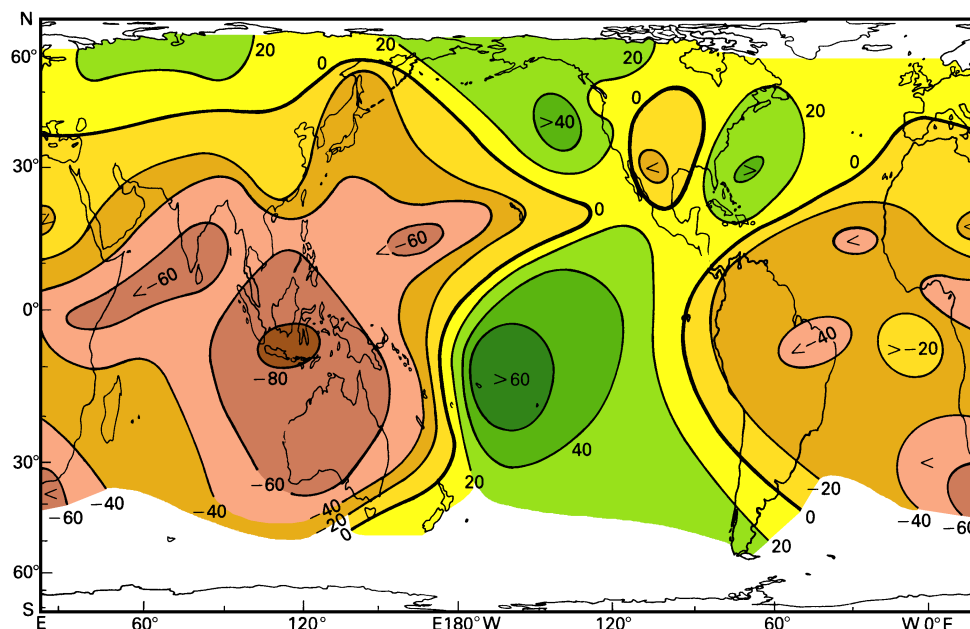


Fig. 19.3. Correlation (%) between air pressure at sea level and the Southern Oscillation Index (for explanation of the index, see text) for December - February. Adapted from Wright (1977).

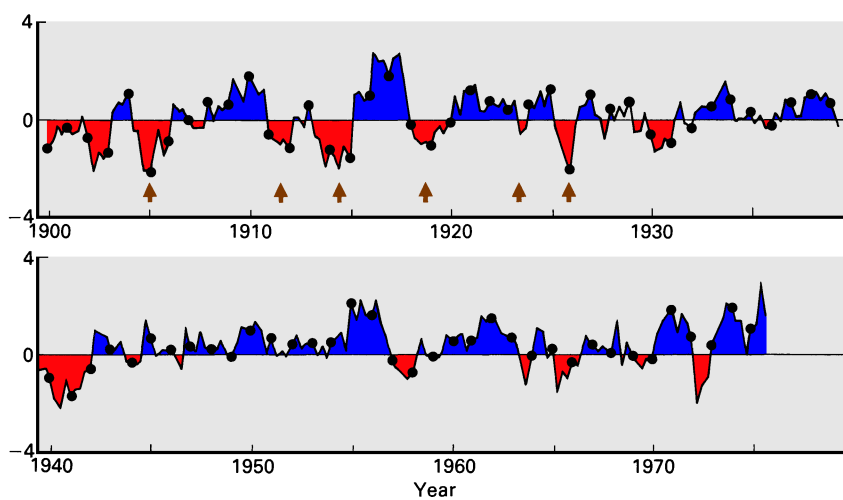


Fig. 19.4. Time series of seasonal values of the Southern Oscillation Index in units of one standard deviation from the mean. Seasons are defined February - April (identified by the dots on the curve), May - July, August - October, and November - January. For an explanation of the index, see text. Arrows identify ENSO events for comparison with Fig. 19.2.

between El Niño and the Southern Oscillation. As an illustration from modern data, Figure 19.6 shows correlation coefficients between sea surface temperature and the Southern Oscillation Index in December - February. It is seen that sea surface temperature is low when the SOI is high (negative correlation) in a broad region of the east Pacific Ocean surrounding Peru; but it is also negative (at this time of year) in the far western Pacific, most of the Indian, and the central South Atlantic Ocean. It is evident that the phenomenon is not restricted to the south Pacific coastal upwelling region but is of global scale.

Fig. 19.5. An example of the effect of El Niño on the biosystem in the upwelling region along the coast of Chile and Peru. annual catch of *anchoveta* (dotted line), number of sea birds, and Southern Oscillation Index (SOI). El Niño events are indicated by arrows on the SOI curve. The 1957 El Niño decimated the bird population. The subsequent build-up of an *anchoveta* fishery resulted in a new competitor and prevented the bird population from recovering to pre-1957 levels. The 1963 and 1965 El Niños affected both competitors, though the bird population suffered more severely. The fishery eventually collapsed to below 3 million tons as a result of overfishing and the 1973 El Niño (see Tomczak (1981a) for more details).

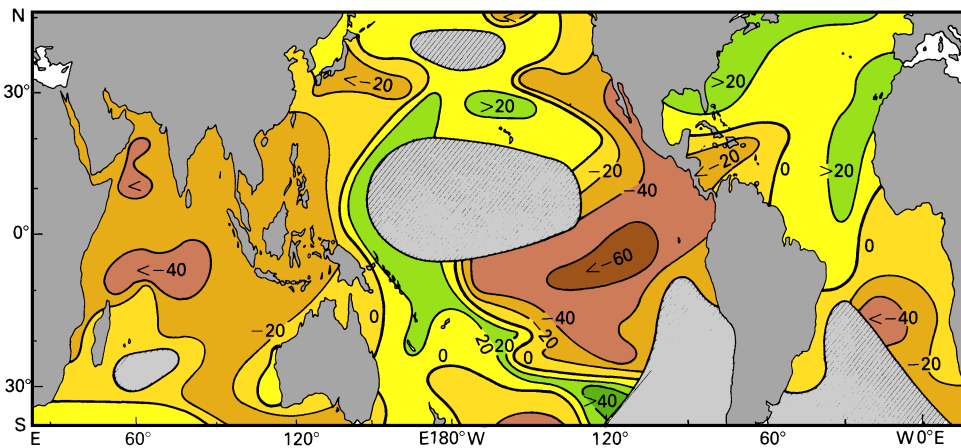
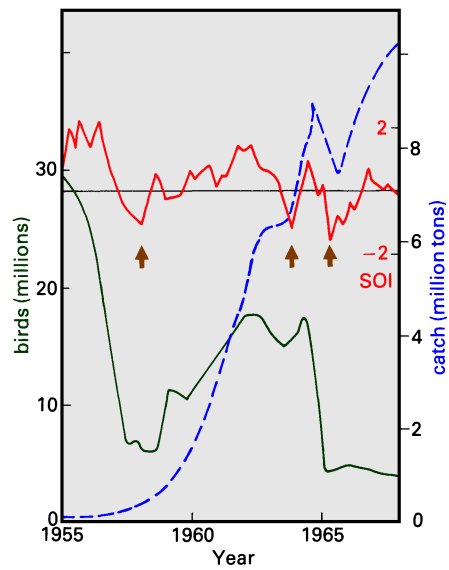


Fig. 19.6. Map of the correlation (%) between sea surface temperature and the Southern Oscillation Index for the December - February season. Data were obtained from merchant vessels along the major shipping routes. Shading indicates regions with no data due to a lack of shipping activity.

deeper density field and therefore the temperature of the water available for upwelling (a particularly important mechanism for SST change in the equatorial east Pacific Ocean, as we shall see). The changed density field alters the geostrophic flow, which also contributes to advection; and finally winds also provide the mechanical energy for stirring deeper water into the mixed layer. A seventh important mechanism for SST change is that due to changes in cloud cover. This plethora of different mechanisms for SST change has meant that, despite considerable progress in recent years, it has not yet been possible to identify a clearly-defined, single mechanism as the trigger for ENSO events. Indeed, there may not be a single dominant mechanism.

However, there is general agreement on one point: Westerly wind bursts in the western Pacific Ocean, i.e. reversals of the general Trade Wind pattern, seem to be a necessary ingredient of the initialization process for an ENSO event. The winds in the equatorial western Pacific Ocean are usually very light; but occasionally an outbreak of westerly winds occurs, perhaps for a week or more at a time, over thousands of kilometers - sometimes along the entire 4000 km stretch from Indonesia to about 170°W. These bursts are linked at their eastward end with pairs of low pressure cells that eventually grow into tropical cyclones (or typhoons, as they are known in the northern hemisphere). Figure 19.8 shows an example of such a situation. The two low pressure cells of 18 May 1986 later separated to lead independent lives as tropical cyclones on either side of the equator.

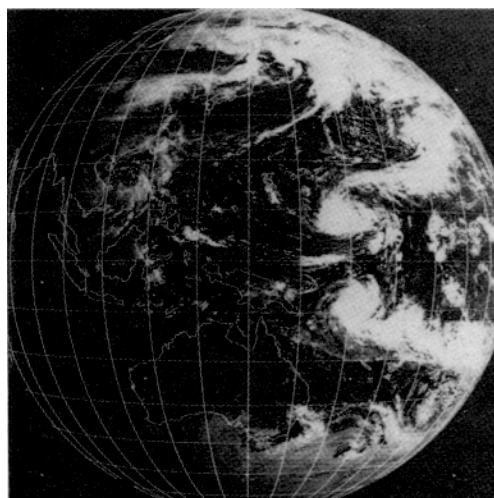


Fig. 19.8. (Right) Cloud cover over the western Pacific Ocean as observed by satellite on 18 May 1986, indicating a tropical cyclone pair in formation near 160°E. (The latitude/longitude grid shows every 10°; the centre longitude is 140°E.) Note the westerly winds at the equator.

These westerly wind bursts are important for setting in train wave motions characteristic for the equatorial region (Figure 19.9). They literally blow surface water eastward along the equator. Because during westerly winds the Ekman transports are directed towards the equator, these wind bursts also deepen the thermocline on the equator. The equatorward Ekman transports are generally confined to the band between about 5°N and 5°S, so the thermocline shallows near 5° - 7° N or S. A strong westerly burst can create thermocline disturbances such as sketched in Figure 19.9b within a few days. These disturbances then begin to move, through the action of equatorial wave dynamics.

and is due to the action of equatorial *Kelvin waves*. The principle of a Kelvin wave propagating along the equator is illustrated in Figure 19.10a. Note that an equatorial Kelvin wave can only move eastwards. Several clear examples of Kelvin wave generation by westerly wind bursts have been seen on Pacific tide gauge records. They travel with little dissipation over the entire width of the Pacific Ocean, about 10 - 20% faster than the predicted speed; the excess speed is due to advection by the Equatorial Undercurrent.

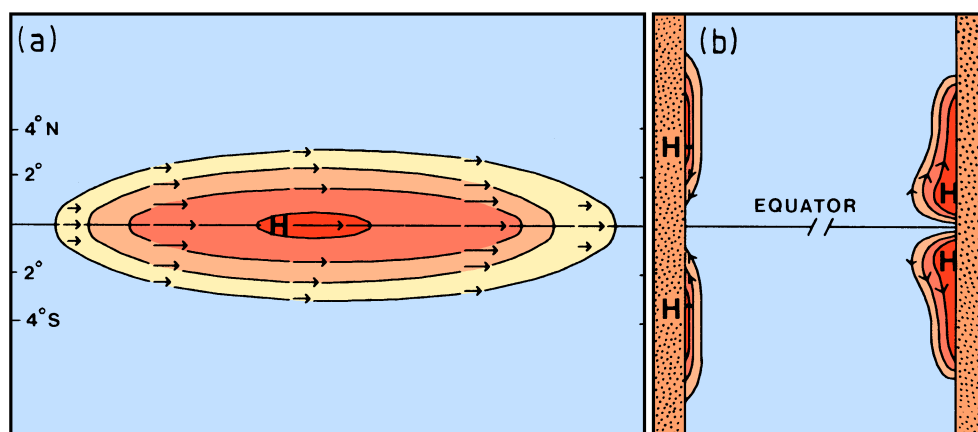


Fig. 19.10. Sketch of Kelvin wave dynamics. (a) For an internal equatorial Kelvin wave, in a $1\frac{1}{2}$ layer ocean; contours indicate upper layer pressure or thermocline depth, arrows show flow direction. An isolated thermocline depression spans the equator; flow is purely zonal, in geostrophic balance and thus eastward on both sides of the equator. This removes thermocline water from the western end of the region and deposits it at the eastern end, resulting in eastward movement. (An isolated patch of *shallow* thermocline also moves eastward, though the currents and pressure gradients both have the opposite signs); (b) for internal Kelvin waves along meridional coastlines. The pressure gradients in the offshore direction are in geostrophic balance; on the western side this implies equatorward flow. This removes thermocline water from the poleward end of the region and deposits it at the equatorward end, resulting in equatorward movement. Rossby wave action keeps these waves tightly confined to the western boundary, i.e. they are disturbances of the western boundary current. Similarly, along the eastern boundary flow is poleward; this removes thermocline water from the equatorward end of the region and deposits it at the poleward end, resulting in poleward movement. In this case the patches can also propagate slowly westward through Rossby wave propagation, resulting in broadening of the pattern, especially near the equator.

After another month or so the patch of shallow thermocline has reached the western boundary and has started to produce a disturbance in the western boundary currents there. This occurs primarily equatorward of the original patch of shallow thermocline (Figure 19.10b). These equatorial disturbances in turn generate new equatorial Kelvin waves which propagate rapidly eastward, this time involving an uplifting of the thermocline (the “nose” of shallow thermocline emanating from the west in Figure 19.9d).

The existence of a positive feedback loop infers that the steady state which corresponds to the long-term mean distributions of the oceanic and atmospheric parameters is rarely, if ever, realized. The combined ocean - atmosphere system is continuously changing, in response to the positive feedback described in Chapter 18. What remains to be discussed is how the system changes from one operational state of the feedback to the other, and why the ENSO state is less frequent than the non-ENSO state. The answer to this question lies in a closer study of the time evolution of an ENSO event. Because individual ENSO events vary widely in intensity and duration, the best data set to produce a somewhat general answer is a "composite" event, i.e. the pattern which shows up in the pre-ENSO, ENSO, post-ENSO, and non-ENSO means. The data base required for such an undertaking has become available over the last three or four decades and was strengthened significantly through an international research programme designed to study ENSO dynamics. The programme, known as TOGA (Tropical Ocean, Global Atmosphere), began in 1985 and will continue into 1994 as part of the World Climate Research Programme (WCRP).

For the purpose of this description, we follow Rasmusson and Carpenter and divide the composite ENSO event into five "phases", the antecedent, onset, peak, transition, and mature phases. Figure 19.11 identifies the phases in relation to the composite ENSO year and the rainfall history at two island locations. It should be noted that there is much variability between different ENSO events, and the composites discussed below are not very useful as a practical forecasting tool. Nevertheless, they provide a frame of reference for studying in broad outline what might be happening during an ENSO event.

Fig. 19.11. Time development of rainfall, expressed in a rainfall index, in Indonesia, near Nauru (167°E), and in the Line Islands (near 160°W), for the composite ENSO event. Antecedent: August - October of pre-ENSO year; onset: November - January; peak: March - May; transition: August - October; mature: December - February of post-ENSO year. All values are three month running means. Note the out-of-phase relationship between Indonesian and Nauru rainfall anomalies, and the eastward propagation of the rain anomaly from Nauru to the Line Islands.

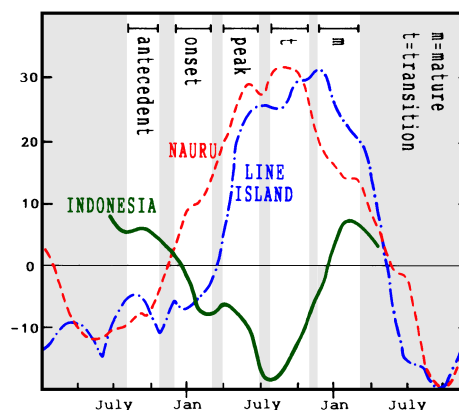


Figure 19.12 shows *anomalies* of near-surface wind vectors and SST for the antecedent phase, in August - October preceding ENSO. The Southwest Monsoon is still active at this time of year, and is stronger than usual, drawing moist air from the Pacific Ocean and thus causing the particularly strong Trades seen in the western equatorial Pacific region. SST values are slightly below the non-ENSO average across most of the equatorial Pacific Ocean, but slightly higher SST occurs near Indonesia and Papua New Guinea, (A in Figure 19.7). Because the mean SST maximum in Figure 19.7 is so broad, this implies an absolute SST maximum near A. Figure 19.11 shows that the high SST near A (Indonesia)

position of the absolute SST maximum eastward towards *B*. The strengthening of the westerlies east of Papua New Guinea is in fact due to an increased frequency of westerly wind bursts. An indication of these bursts can be seen in the composite mean as well (Figure 19.13): the wind anomalies near 170°E show a tendency for tropical cyclone pair formation near 170°E (anti-clockwise north, clockwise south of the equator).

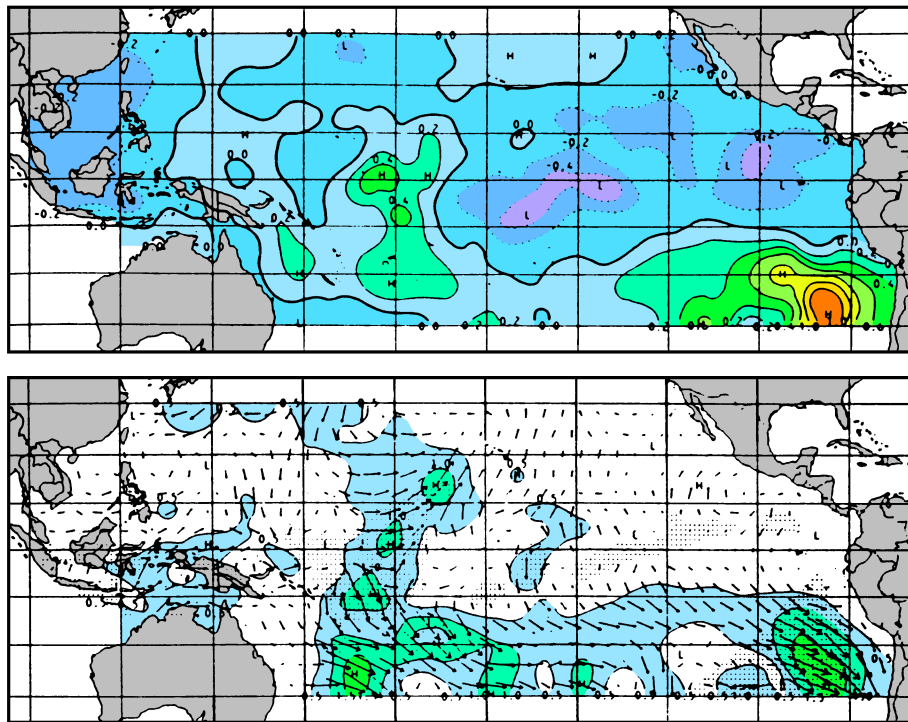


Fig. 19.13. SST anomaly (°C) and wind anomaly (m/s), during the onset phase of ENSO (November - January). For details see Fig. 19.12. From Rasmusson and Carpenter (1982).

What appears to be happening at this time of development of an ENSO event is that, associated with the strong Australian monsoon, a new convection centre forms near *B*. It competes with the more usual convection centre near *A*, sucking westerly winds towards it. We have noted that the very small SST changes from Figure 19.12 to Figure 19.13 are in fact enough to displace the very broad SST maximum from near *A* in Figure 19.7 to near *B*, so the new convection centre near *B* is consistent with the principle that convection over the Pacific Ocean follows SST maxima. Note that mean rainfall west of the date line is uniformly large (about 3 m per year from Indonesia to Nauru), so a modest fractional change in rainfall at either place is a very big change in absolute terms. The reduction of rain over Indonesia and accompanying increase over Nauru is apparent in Figure 19.11.

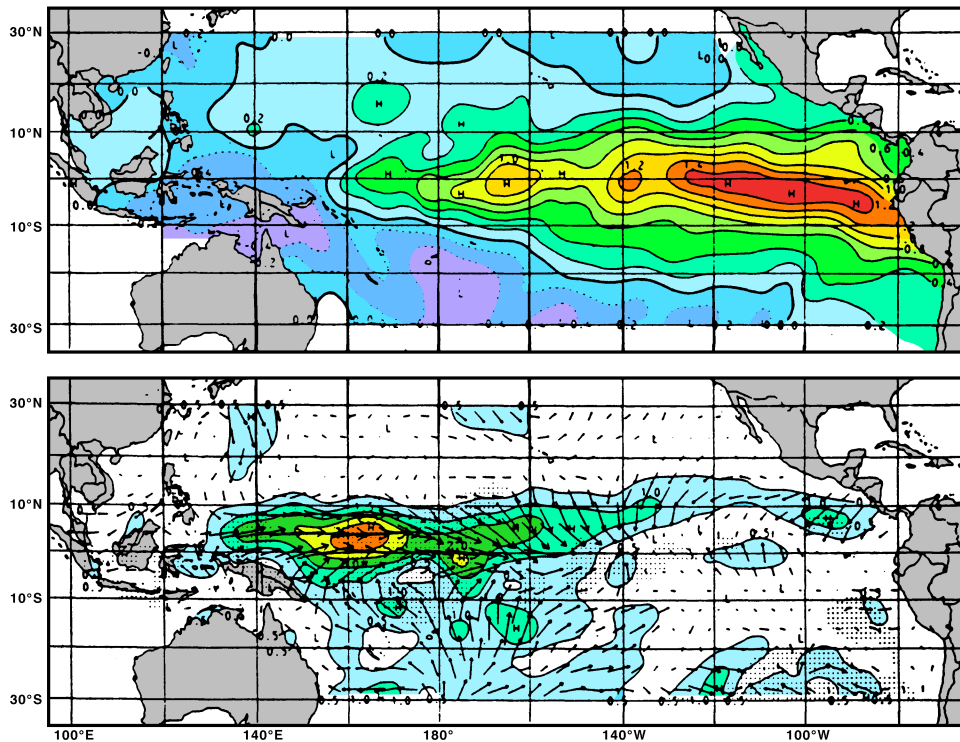


Fig. 19.15. SST anomaly ($^{\circ}\text{C}$) and wind anomaly (m/s), during the transition phase of ENSO (August - October). For details see Fig. 19.12. From Rasmusson and Carpenter (1982).

The ENSO event usually does not break until the next change of season (December - February following El Niño), when the winds are disturbed throughout most of the Northern Hemisphere over the Pacific Ocean (Figure 19.16). A significant positive SST anomaly develops in the South China Sea and the Indonesian waters, attracting the winds from the far western Pacific Ocean which begin to blow strongly towards it, breaking the drought there, and the Trades are strong again in the west Pacific region. The east Pacific SST anomaly dies shortly thereafter.

The above description of an ENSO event places strong emphasis on the small SST anomalies in the western Pacific rather than the much more dramatic ones in the eastern Pacific Ocean, because they shift the SST maximum and hence the convection patterns to the central Pacific region. Strong support for the relative importance of the small SST anomalies in the west for ENSO comes from sensitivity tests with atmospheric models which show that a change of SST in the east affects the wind field much less than a corresponding SST change in the west. This suggests that our skills in predicting ENSO events should be closely tied to our ability to forecast very small SST changes in the western Pacific Ocean. In this region, as we have seen, the equatorial Kelvin waves do not play a dominant role in SST change; local changes in surface heat fluxes — solar radiation and evaporative heat loss — are sufficient to account for the observed SST changes in the

oceans and the global atmosphere as a time dependent system in order to determine the extent to which the system is predictable on time scales of months to years and to understand the mechanisms and processes underlying its predictability". This aim is tackled with a variety of instrumentation (Figure 19.17 shows some components of the station network in the Pacific Ocean; others include island tide gauge installations and oceanographic satellites). TOGA is increasingly seen as a forerunner of a permanent oceanic observation network analogous to the network of meteorological observation stations on land. As in meteorology, success in forecasting climate variability will be achieved by transmitting the data to information processing centres in real time and assimilating them into numerical models of the oceanic and atmospheric circulation. The planning for the Global Ocean Observing System (GOOS) began in 1992.

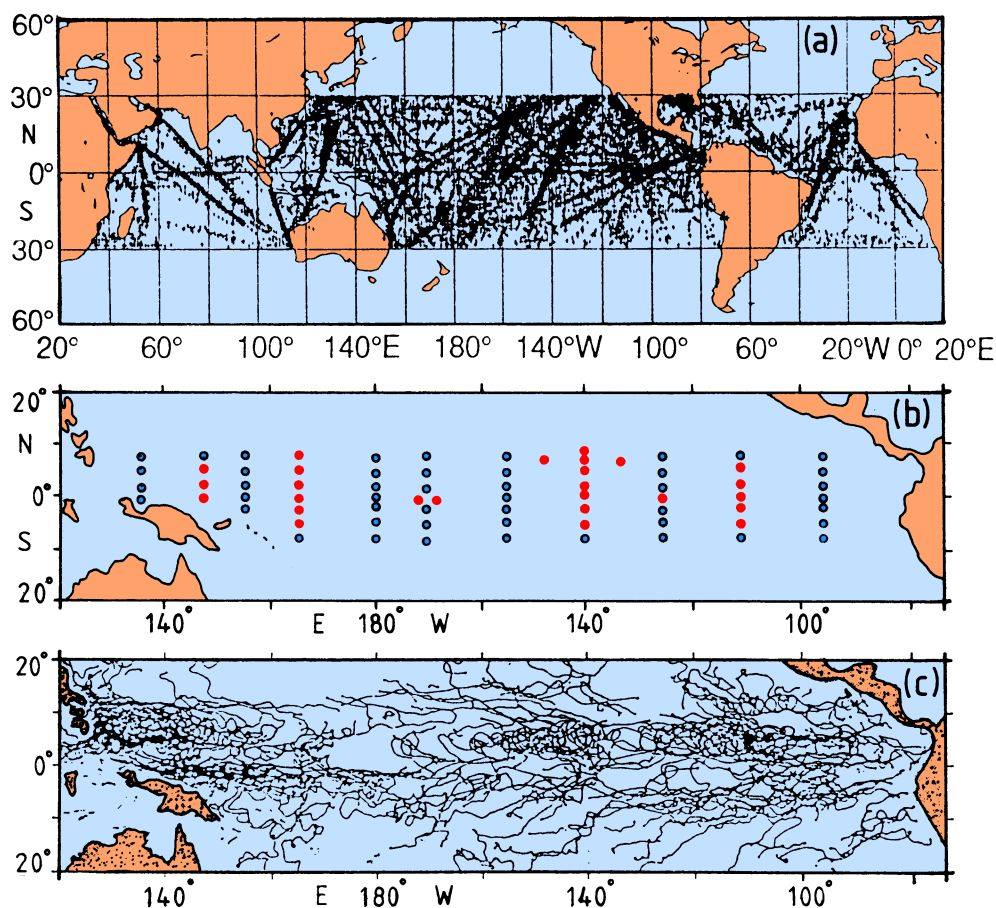


Fig. 19.17. Some of the observation components of TOGA. (a) Station positions where temperature profiles for 0 - 450 m depth, using expendable instrumentation, were obtained by merchant vessels during 1987; (b) existing (dots) and planned (1994, circles) arrays of current meter moorings; (c) trajectories of TOGA surface drifters for July 1988 - February 1990.

Ocean. (top) June 1983, (bottom) June 1984. From Philander (1990).

Figure 19.18 shows the sea surface temperature for June 1983 and twelve months later. While temperatures in the two upwelling regions outside the 20°S - 20°N equatorial belt showed little change over the period, the water within 500 km either side of the equator east of 15°W was anomalously cold in 1983 and anomalously warm in 1984. The 1983 situation was accompanied by dry conditions in northeastern Brazil, strong equatorial Trades, and a continuation of strong upwelling in the northern part of the Benguela Current upwelling system (which usually retreats southward during this time of year). In the following year, westward flow in the equatorial current system was nearly halted, and an intrusion of tropical water similar to that observed along the coast of Peru during El Niño years dominated the northern part of the Benguela Current upwelling system, leading to a temperature increase of 3°C in the upper 50 m of water near 23°S. The causes for such extreme situations in the Atlantic Ocean are not clear. There is also uncertainty about the frequency of their occurrence; only two intrusions of tropical water have been documented for the 40 year period between 1950 and present, although historical records of coastal water temperatures from Namibia seem to indicate one intrusion for every ten years.